Title

Pacific-Antarctic-Australia motion and the formation of the Macquarie Plate

Journal

Geophysical Journal International, 157(1)

ISSN

0956-540X

Authors

Cande, Steven C

Stock, Joann M

Publication Date

2004-04-01

Peer reviewed

Geophys. J. Int. (2004) **157,** 399–414 doi: 10.1111/j.1365-246X.2004.02224.x

Pacific–Antarctic–Australia motion and the formation of the Macquarie Plate

Steven C. Cande[1] and Joann M. Stock[2]

[1] *Scripps Institution of Oceanography, Mail Code* 0220, *La Jolla,* CA 92093-0220, *USA. E-mail: scande@ucsd.edu*
[2] *California Institute of Technology, Mail Stop* 252-21, *Pasadena,* CA 91125, *USA. E-mail: jstock@seismo.gps.caltech.edu*

Accepted 2003 December 15. Received 2003 November 25; in original form 2002 November 25

SUMMARY

Magnetic anomaly and fracture zone data on the Southeast Indian Ridge (SEIR) are analysed in order to constrain the kinematic history of the Macquarie Plate, the region of the Australian Plate roughly east of 145°E and south of 52°S. Finite rotations for Australia–Antarctic motion are determined for nine chrons (2Ay, 3Ay, 5o, 6o, 8o, 10o, 12o, 13o and 17o) using data limited to the region between 88°E and 139°E. These rotations are used to generate synthetic flowlines which are compared with the observed trends of the easternmost fracture zones on the SEIR. An analysis of the synthetic flowlines shows that the Macquarie Plate region has behaved as an independent rigid plate for roughly the last 6 Myr. Finite rotations for Macquarie–Antarctic motion are determined for chrons 2Ay and 3Ay. These rotations are summed with Australia–Antarctic rotations to determine Macquarie–Australia rotations. We find that the best-fit Macquarie–Australia rotation poles lie within the zone of diffuse intraplate seismicity in the South Tasman Sea separating the Macquarie Plate from the main part of the Australian Plate. Motion of the Macquarie Plate relative to the Pacific Plate for chrons 2Ay and 3Ay is determined by summing Macquarie–Antarctic and Antarctic–Pacific rotations. The Pacific–Macquarie rotations predict a smaller rate of convergence perpendicular to the Hjort Trench than the Pacific–Australia rotations. The onset of the deformation of the South Tasman Sea and the development of the Macquarie Plate appears to have been triggered by the subduction of young, buoyant oceanic crust near the Hjort Trench and coincided with a clockwise change in Pacific–Australia motion around 6 Ma. The revised Pacific–Australia rotations also have implications for the tectonics of the Alpine Fault Zone of New Zealand. We find that changes in relative displacement along the Alpine Fault have been small over the last 20 Myr. The average rate of convergence over the last 6 Myr is about 40 per cent smaller than in previous models.

Key words: Alpine Fault, diffuse deformation, Hjort Trench, Macquarie Ridge, South Tasman Sea, Southeast Indian Ridge.

INTRODUCTION

Recent studies have shown that the Indo-Australian Plate is actually a composite of three smaller rigid plates, the Capricorn, Indian and Australian plates, separated by broad diffuse deformation zones (Weissel *et al.* 1980; Wiens *et al.* 1985; DeMets *et al.* 1994; Royer & Gordon 1997). A likely candidate for another section of the Indo-Australian Plate that behaves as a small rigid plate is the region roughly east of 145°E and south of 52°S (labelled MQ in Fig. 1). Several studies have noted that the azimuths of the transform faults on the Southeast Indian Ridge (SEIR) east of 140°E are not consistent with the Euler pole that fits the transforms from the central section of the SEIR (DeMets *et al.* 1988; Kubo *et al.* 1998; Conder & Forsyth 2000). In addition there is a broad zone of intraplate seismicity within the South Tasman Sea, between roughly 50°S and 55°S and between 145 °E and the Macquarie Ridge (the location of the epicentres are shown by plus marks in Fig. 1), that might reflect a diffuse plate boundary (Das 1992; Valenzuela & Wysession 1993). However, it has not been known how much deformation may have taken place, over what time interval, and whether any part of this region has been behaving as a separate rigid plate. For example, in Gordon's (2000) recent study of diffuse oceanic plate boundaries, the entire salient portion of the Australian Plate is portrayed as deforming lithosphere. Although DeMets *et al.* (1988) considered the tectonic history of the region problematical, they proposed the name Macquarie Plate for the region.

Defining the kinematics of the Macquarie Plate is important because this region interacts with the Pacific Plate across the

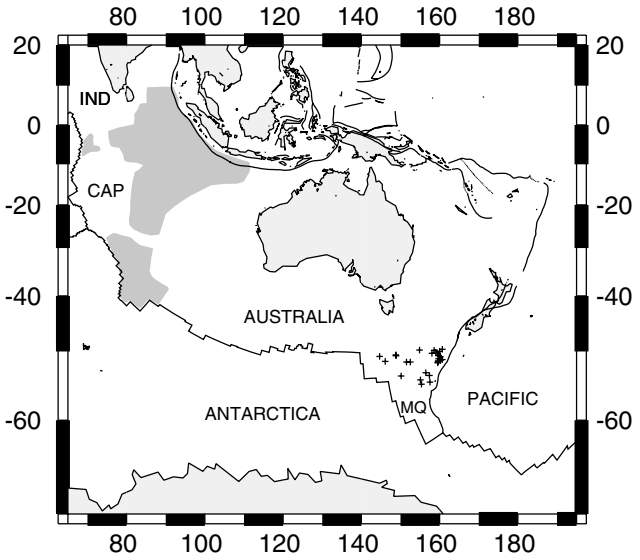

Figure 1. Location of the Macquarie Plate (MQ). Other component parts of the Indo-Australian Plate include the Capricorn (CAP) and Indian (IND) plates. Dark shaded regions are zones of diffuse deformation. Epicentres of intraplate earthquakes in the South Tasman Sea from Valenzuela & Wysession (1993) are shown by crosses.

Macquarie Ridge and Hjort Trench. There are several outstanding tectonic issues related to this interaction. For example, global plate motion models (e.g. DeMets *et al.* 1994) predict a large component of convergence across the Hjort Trench yet earthquake focal mechanisms (Frohlich *et al.* 1997; Ruff *et al.* 1989) indicate that the current plate motion is largely strike-slip. The dimensions of preserved conjugate-age seafloor on the Australian and Antarctica plates in the region require that upwards of 200 km of the Australian Plate has been subducted beneath the Macquarie Ridge and Hjort Trench over the last 20 Myr (Weissel *et al.* 1977), yet there is little evidence along the central part of the Macquarie Ridge for this amount of subduction (Massell *et al.* 2000). There are also tectonic questions related to the mechanism by which larger plates deform and smaller regions develop as rigid subplates. In the case of the Capricorn, Indian and Australian plates it has been shown that the Euler poles defining their relative motion lie within the deformation zone separating the rigid plates (Royer & Gordon 1997; DeMets *et al.* 1994), an observation that has important implications for plate tectonic theory (Gordon 1998; Zatman *et al.* 2001). A similar situation may exist for the Macquarie Plate.

The tectonic setting of the Macquarie Plate has remained enigmatic, in large part due to the paucity of shipboard geophysical data in the region. There are no systematic surveys of any of the large fracture zones along the eastern part of the SEIR and not even the transform azimuths are known with any degree of accuracy. In addition, the kinematics of the SEIR have not been studied in detail. The youngest published rotation for Australia–Antarctic motion that uses data from the entire boundary, other than the 'instantaneous' NUVEL-1A datum (DeMets *et al.* 1994), is for Chron 5o (Royer & Gordon 1997). However, developing a detailed kinematic model for the region requires knowing the motion of the Australian and Antarctic plates at an interval of 3 or 4 Myr in the Late Miocene as well as plate rotations at coarser time intervals back to the Early Cenozoic.

In this paper, we calculate rotation parameters for nine anomalies on the SEIR using data limited to the region between 88°E and 139°E. This area corresponds to the ocean crust that was generated at the boundary between the Antarctic Plate and the main part of the Australian Plate and thus avoids complexities related to the Capricorn Plate and to the enigmatic azimuths of the eastern transform faults. We use the rotations to calculate synthetic flowlines for Australia–Antarctic motion which we then compare with the observed trends of the easternmost fracture zones on the SEIR, the Balleny and Tasman fracture zones. From an analysis of these synthetic flowlines we are able to show that the region south of the zone of intraplate seismicity in the South Tasman Sea, approximately corresponding to the Macquarie Plate of DeMets *et al.* (1988), appears to have acted as a separate rigid plate since roughly 6 Ma. In addition, we show that the magnetic anomaly and fracture zone observations are consistent with a kinematic model in which the Macquarie Plate has rotated with respect to Australia about a pole located within the diffuse deformation zone. The revised SEIR rotations also enable us to examine the possible cause of the onset of deformation.

REVISED AUSTRALIA–ANTARCTIC FINITE ROTATION PARAMETERS

The motion of Australia with respect to Antarctica has been the subject of several studies over the last 30 yr. Weissel & Hayes (1972) first calculated rotation parameters for Australia–Antarctic at roughly 10 Myr intervals (anomalies 5, 6, 8, 13 and 22) using shipboard magnetic and bathymetric data. Royer & Sandwell (1989) used gravity constraints from satellite altimetry measurements to refine the SEIR rotations but still at roughly 10 Myr intervals. In an analysis of the tectonic history of the Australia–Antarctic Discordance (AAD), Marks *et al.* (1999) determined SEIR rotations at roughly 3 Myr intervals from 19 Ma to the present. However, since they were focused on constraining motion within the AAD, they only used data from a short section of the SEIR. Consequently, the uncertainty ellipses for their rotations are large. As part of a study of the Capricorn Plate, Royer & Gordon (1997) calculated a revised Chron 5o rotation for Australia–Antarctic spreading. Although a well-constrained rotation, this rotation by itself is insufficient to define the Late Miocene spreading history of the SEIR.

We calculated finite rotation parameters for Australia–Antarctic motion for nine chrons (2Ay, 3Ay, 5o, 6o, 8o, 10o, 12o, 13o and 17o, where 'y' refers to the 'young end' of the normal polarity interval and 'o' refers to the 'old end') using archival magnetic anomaly data and fracture zones constrained from the satellite-derived gravity field of Sandwell & Smith (1997). The ages of these points as given in the timescale of Cande & Kent (1995) are included in Table 1. The magnetic anomaly data were obtained from the archives of the Geological Data Center at the Scripps Institution of Oceanography, the National Geophysical Data Center (NGDC), the Indian Ocean Data Compilation Project (Sclater *et al.* 1997) and the Japanese Geological Survey (Takemi Ishihara, personal communication, 1997). We followed the precedent set by Royer & Gordon (1997) and only used data between 88°E and 139°E to constrain the rotations.

Fig. 2 shows the magnetic anomaly and fracture zone locations that were used in this study. The magnetic anomaly locations were digitized from Mercator plots of magnetic profiles along track, using model profiles constructed for the latitude and longitude of the data in order to compensate for the skewing effect of non-vertical geomagnetic inclinations. The fracture zone locations were digitized from Mercator plots of the satellite-derived gravity data of Sandwell

Table 1. Finite rotations of Australia relative to Antarctica.

Chron	Age (Ma)	Lat (° N)	Long (°E)	Angle (deg)	Mag Pts	FZ Pts	Mag Segs	FZ Segs
2Ay	2.58	−11.164	−139.700	1.655	61	37	10	4
3Ay	6.04	−11.591	−139.230	3.830	70	42	11	6
5o	10.95	−11.896	−142.058	6.790	81	41	8	6
6o	20.13	−13.393	−145.630	12.051	96	36	9	6
8o	26.55	−13.805	−146.444	15.919	85	30	11	5
10o	28.74	−13.580	−146.016	17.319	71	27	11	4
12o	30.94	−13.396	−145.623	18.890	70	19	10	3
13o	33.54	−13.451	−145.623	20.495	66	30	10	5
17o	38.13	−14.650	−146.525	22.882	42	7	7	1

Ages are from Cande & Kent (1995) except for 3Ay which is from Krijgsman *et al.* (1999). Mag Pts and FZ Pts = the total number of magnetic anomaly and fracture zone points, respectively. Mag Segs and FZ Segs = the number of segments with magnetic anomaly and fracture zone data, respectively.

& Smith (1997). The selection of a specific point to digitize on the roughly 20 to 40 km wide gravity signature that straddles most fracture zones is problematical. At moderate to fast spreading rates the offset appears to coincide with the steepest gradient in the gravity field (e.g. Sandwell & Schubert 1982), but at slower spreading rates the location of the offset appears to correspond to a low in the gravity field centred over a trough in the bathymetry (e.g. Müller & Roest 1992; Cande *et al.* 1995). This observation is relevant to the SEIR since there was an increase in spreading rate on the SEIR around Chron 3Ay (Cande & Kent 1995 ; Krijgsman *et al.* 1999). By comparing shipboard bathymetric data and satellite gravity data in several different locations we found that, in general, on the SEIR the fracture zone offset coincides with the trough of the gravity signature except near the ridge where the offset appears to be more closely coincident with the steepest gradient. Consequently, we digitized fracture zone offsets at locations corresponding to gravity lows except for chrons 2Ay and 3Ay for which we digitized points corresponding to the steepest gradient.

We followed the method of Hellinger (1981) and determined reconstruction parameters by dividing the data into multiple segments and fitting great circles to the reconstructed data in each segment. The magnetic anomalies and fracture zones were used to define up to 17 segments. We used the best-fitting criteria and statistical techniques of Chang (1987, 1988) and Royer & Chang (1991) to calculate rotation parameters and estimate uncertainty ellipses. This method requires that an estimate of the error in the position be assigned to every data point. Although it is possible to assign a separate error estimate to each data point, varying it, for example, for the type of navigation, this level of detail was beyond the scope of this study. Instead, based on our experience with other data sets,

Figure 2. Magnetic anomaly locations and fracture zone crossings used to constrain the Australia–Antarctic finite rotations determined in this paper. Anomalies 2Ay, 8o and 17o are denoted by circles, 3Ay and 10o by triangles, 5o and 12o by squares and 6o and 13o by diamonds. Open symbols are unrotated anomalies; filled symbols have been rotated from the conjugate plate.

Table 2. Covariance matrices for finite rotations in Table 1.

Chron	$\hat{\kappa}$	*a*	*b*	*c*	*d*	*e*	*f*	*g*
2Ay	5.33	2.81	−3.35	2.60	5.15	−4.87	9.06	7
3Ay	2.12	2.94	−3.90	3.19	6.27	−5.83	8.97	7
5o	1.02	1.36	−1.71	0.556	3.05	−1.89	4.47	7
6o	1.06	1.61	−1.85	0.265	3.00	−1.59	4.22	7
8o	1.01	1.95	−2.24	0.579	3.71	−2.39	5.90	7
10o	1.17	2.32	−2.56	0.848	3.94	−2.77	7.51	7
12o	0.75	2.60	−3.14	0.553	5.18	−3.10	9.82	7
13o	1.07	2.44	−3.26	1.49	5.56	−3.43	6.93	7
17o	0.49	6.88	−8.39	−2.51	13.4	−1.37	13.1	7

The covariance matrix is given by the formula

$$\frac{1}{\hat{\kappa}} * \begin{pmatrix} a & b & c \\ b & d & e \\ c & e & f \end{pmatrix} \times 10^{-g}$$

where the values of a–f are given in radians squared.

we assigned an average estimate of 4 km for all magnetic anomaly points and 10 km for all fracture zone crossings.

As part of the solution using the Chang (1987, 1988) method a statistical parameter, $\hat{\kappa}$, is returned which is an evaluation of the accuracy of the assigned errors in the location of the data points. If $\hat{\kappa}$ is near 1, the errors have been correctly assigned; if $\hat{\kappa}$ is $\gg 1$ the errors are overestimated; and if $\hat{\kappa}$ is $\ll 1$ the errors are underestimated. For most of our data sets, the value of $\hat{\kappa}$ was near 1, indicating that the error estimates were reasonable. For chrons 2Ay and 3Ay the values of $\hat{\kappa}$ were 5.3 and 2.1 indicating that the error values were overestimated by a factor of 2.3 and 1.45, respectively (i.e. by the $\sqrt{\hat{\kappa}}$) while for chrons 12o and 17o the $\hat{\kappa}$ values were 0.6 and 0.5 indicating that the errors were underestimated by a factor of 0.77 and 0.71 respectively. Although a $\hat{\kappa}$ of 1.0 could be obtained by dividing the original error estimates by $\sqrt{\hat{\kappa}}$, this rescaling makes no difference in the location of the poles and only a minor difference in the size of the uncertainty ellipses for all of these chrons. Consequently, for the sake of consistency, we cite the results using the original error estimates. The error estimates are implicitly rescaled later in the paper when the Australia–Antarctic rotations are combined with Antarctic–Macquarie and Antarctic–Pacific rotations.

The best-fit parameters and covariance matrices for the nine rotations are given in Tables 1 and 2, respectively. Table 1 also documents the data that were used to constrain each rotation, giving the number of segments and the number of points for each data type. The best-fit rotation poles with their 95 per cent uncertainty ellipses are shown in Fig. 3. We also plot the locations of the NUVEL-1A pole for the Australia–Antarctic ridge (DeMets *et al.* 1994), the Royer & Gordon (1997) Chron 5o pole and the Conder & Forsyth (2000) 1 Ma pole. As a demonstration of the total data coverage that forms the basis for this study, in Fig. 2 we have used the new rotation parameters to rotate the data points from the Antarctic Plate back to their predicted location on the Australian Plate, and those from the Australian Plate to their predicted location on the Antarctic Plate. The rotated and non-rotated data points are shown by filled and open symbols respectively.

MAGNETIC ANOMALY AND FRACTURE ZONE CONSTRAINTS ON THE MACQUARIE PLATE

The new Australia–Antarctic rotation parameters enable us to estimate the amount of deformation in the region of the SEIR east of 140°E and also to determine whether some portion of this region has acted as a rigid plate. We first examined the predicted fit of magnetic anomalies and fracture zones between the George V FZ and the Macquarie Triple Junction (MTJ). In Fig. 4 we show magnetic anomalies 2Ay, 3Ay, 5o, 6o and 8o from the Australia and Antarctic plates east of the George V fracture zone (FZ) rotated back to their conjugate locations on the Antarctic and Australian plates respectively. As with Fig. 2, the filled symbols are points from the Antarctic Plate rotated back to the Australian Plate or points from the Australian Plate rotated to the Antarctic Plate. Fig. 4 shows that there is no apparent misfit of the magnetic anomalies between the

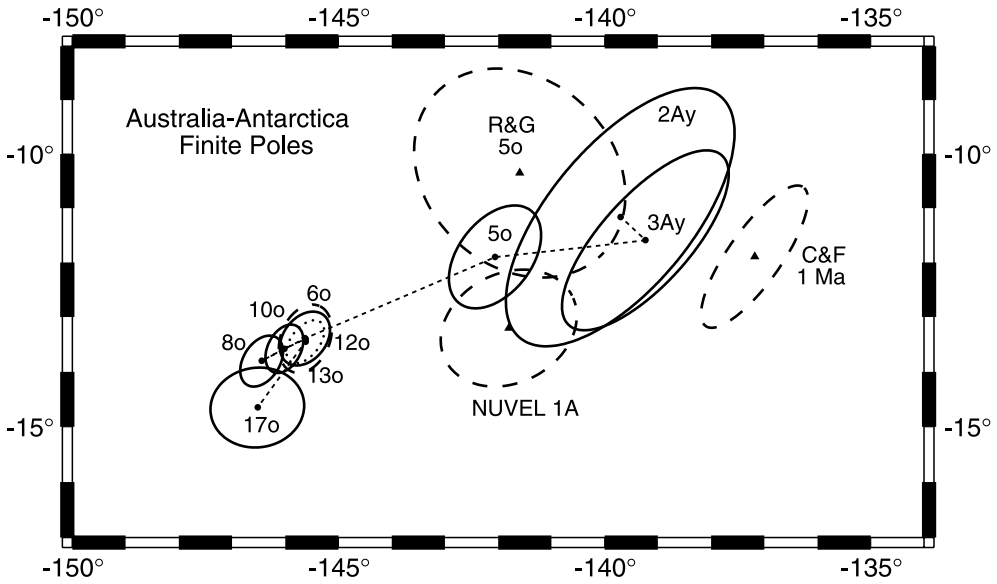

Figure 3. Australia–Antarctic finite rotation poles. The poles determined in this paper are shown by filled circles and connected by a dotted line. The 95 per cent confidence ellipses for these rotations are indicated by solid lines except, for clarity, the Chron12o ellipse is shown by a dashed line and the Chron 13o ellipse by a dotted line. R&G/5 indicates the best-fit Chron 5o pole of Royer & Gordon (1997). C&F/1Ma marks the 1 Ma pole of Conder & Forsyth (2000). The NUVEL-1A pole is from DeMets *et al.* (1994).

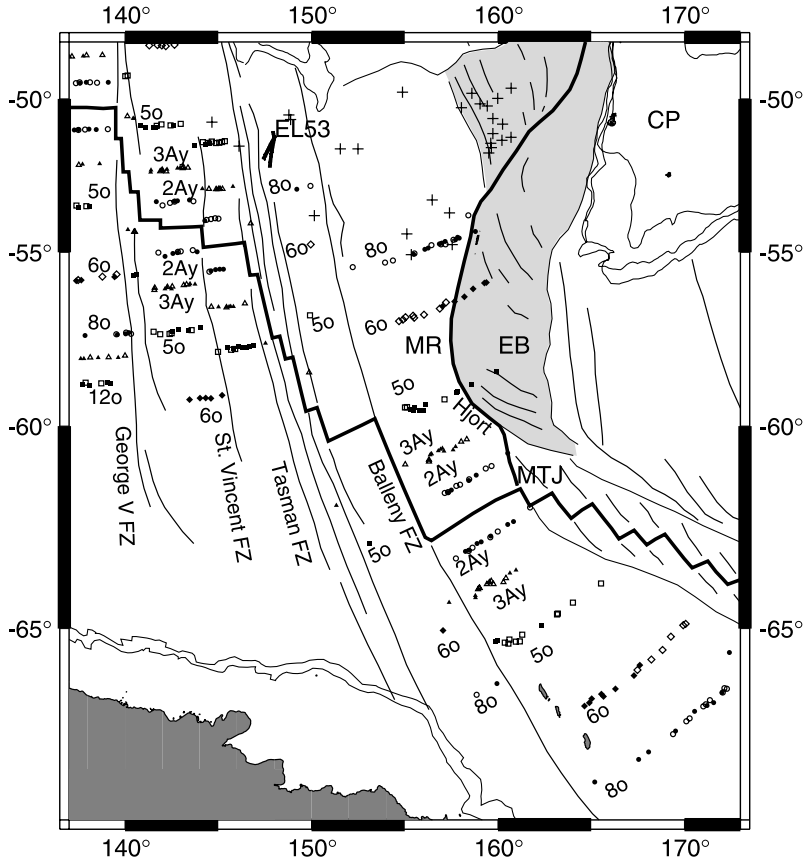

Figure 4. Demonstration of the fit of magnetic anomalies east of the George V FZ when rotated by the Australia–Antarctic rotations based only on data west of the George V FZ. The rotated anomalies (filled symbols) all overlie their opposite plate counterparts reasonably well with no across-isochron misfit. However, the Antarctic Plate anomalies east of the Balleny FZ are shifted by up to 50 km to the east along the strike of the Australian lineations. The misfit is not that obvious here because there are few data from near the Balleny FZ, but it is made clearer in Fig. 5. The shaded region near the Macquarie Ridge shows the oceanic crust generated by Australia–Pacific spreading between roughly 45 and 20 Ma. EL53 marks the location of the *Eltanin* 53 profiles (heavy lines) discussed in the text. MR = Macquarie Ridge, MTJ = Macquarie Triple Junction, EB = Emerald Basin, CP = Campbell Plateau.

George V FZ and the Tasman FZ. In fact, the average misfit of the anomalies in these segments is about the same as for the segments in the central part of the SEIR. The rotated anomaly points east of the Balleny FZ also appear to overlie their Australian or Antarctic plate counterparts. However, here there is a significant misfit in as much as the anomalies from the Antarctic Plate are rotated too far to the northeast, along the strike of the Australian Plate isochrons. This can be seen more clearly in Fig. 5 in which we have digitized points from the intersection of the Balleny FZ and isochrons for anomalies 2Ay, 3Ay and 5o on the Antarctic Plate and rotated them back to the Australian Plate. The rotated points, with their uncertainty ellipses, are clearly mislocated by up to 50 km to the northeast of the Balleny FZ, along the strike of the isochron.

An effective way to demonstrate the deviation of the trends of the Tasman and Balleny FZs from true Australia–Antarctic spreading, as Fig. 5 suggests, is to compare the observed fracture zones to synthetic flowlines. Synthetic flowlines are generated by starting from points at conjugate ridge-transform intersections and using the stage rotations to predict the motion of each plate as it moves away from the ridge at the half spreading rate. Synthetic flowlines based on the new rotation parameters should parallel the observed fracture zones. As a demonstration, in Fig. 6 we show synthetic flowlines for the major fracture zones along the central portion of the SEIR. These flowlines were calculated using the rotations in Table 1 augmented by a Chron 20o rotation from Tikku & Cande (1999). All of the fracture zones between 80°E and 145°E, including fracture zones not included in the data set constraining the rotations (e.g. the Vlamingh and Geelvinck FZs to the west and the George V and St Vincent FZs to the east; Fig. 6), are well matched by the synthetic flowlines. However, the middle and eastern splays of the Tasman FZ and the Balleny FZ deviate significantly from the synthetic flowlines, as is shown in Fig. 7(a). The misfit is particularly apparent on the Antarctic Plate. The synthetic flowlines cut across the grain of the fracture zones for 200 km and are not solidly on track, paralleling the fracture zones, until around anomaly 3Ay. However, south of anomaly 3Ay, the synthetic flowlines parallel the fracture zones all the way south to the Antarctic margin. On the Australian side of the ridge the misfit is more complicated. The synthetic flowlines deviate slightly to the east of the Tasman East and Balleny FZs for the first 200 or 300 km going north from the ridge, but then cross the fracture zones near 57°S and gradually deviate up to 30 km on the west side of the observed fracture zones.

Understanding the fracture zone misfit is fundamental for developing a kinematic model for the region. At this point, if we ignore the intraplate seismicity between 50°S and 55°S on the Australian Plate, there is no *a priori* reason to assume that the fracture zone misfits are due to deformation within the Australian Plate instead of the Antarctic Plate. For example, the occurrence of a magnitude 8.2 intraplate earthquake and its aftershocks on the Antarctic Plate along a line stretching from the George V FZ to the Tasman FZ

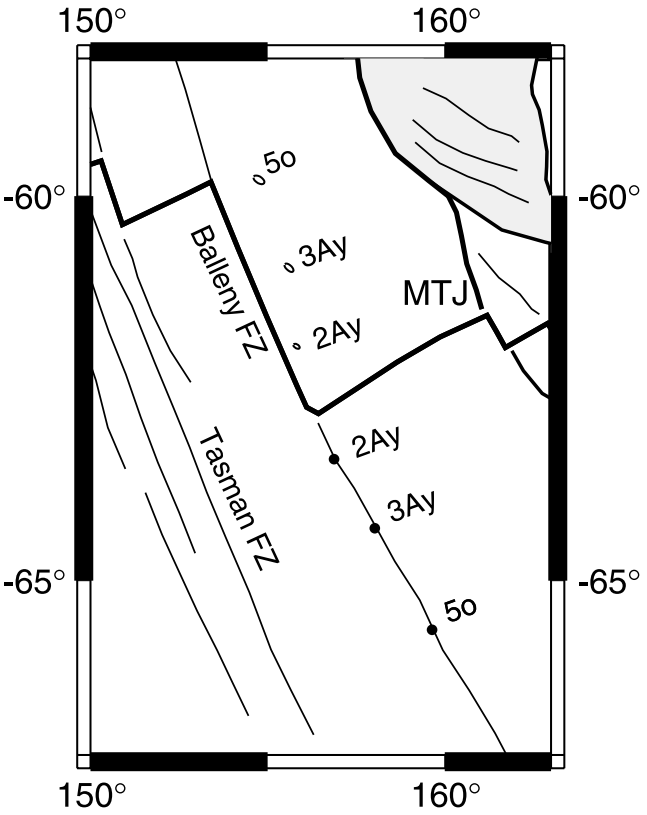

Figure 5. Demonstration of the misfit east of the Balleny FZ produced by the Australia–Antarctic rotations. Three points on the Antarctic Plate corresponding to the intersection of the Balleny FZ and the 2Ay, 3Ay and 5 lineations (solid circles) have been rotated back to the Australian plate (small ellipses). The rotated points fall up to 50 km east of the Balleny FZ. The ellipses show the 95 per cent uncertainty in the predicted location of the rotated points. MTJ = Macquarie Triple Junction.

near 63°S (Nettles *et al.* 1999; Henry *et al.* 2000) might indicate a missing plate boundary between East and West Antarctica. Although Conder & Forsyth (2000) showed that the focal mechanism from this earthquake did not fit the expected sense of motion for a 'Balleny Plate' located south of the SEIR, it is possible that a boundary continued elsewhere on the Antarctic Plate. Eliminating this possibility is an important step.

We found that shifting the synthetic flowlines shown in Fig. 7a roughly 30 km to the northeast, orthogonal to the transform direction, was a very revealing exercise. In Fig. 7(b) these 'offset' flowlines are compared with the Balleny and Tasman FZs. As expected from Fig. 7(a), the offset flowlines agree very well with the FZs on the Antarctic Plate starting around anomaly 3Ay, about 200 km south of the spawning point. Further south, the synthetic flowlines match the observed fracture zones all the way back to anomaly 20. On the Australian side of the ridge, the flowlines are displaced to the east of the observed fracture zones north to about 54°S or 55°S, but farther north they actually fit the observed fracture zones quite well.

We interpret the observations that the misfit of the fracture zones is worse on the Australian Plate and that the misfit affects older crust on the Australian Plate, as strongly supporting the contention of DeMets *et al.* (1988) that the intraplate deformation is occurring on the Australian Plate, and not the Antarctic Plate. Furthermore, since the Antarctic Plate FZs fit the SEIR motion except for the region younger than roughly anomaly 3Ay, the deformation appears to have started around 6 Ma. This pattern is consistent with a rigid clockwise rotation of the region south of roughly 55°S, the Macquarie Plate, which is separated from the main part of the Australian Plate by diffuse deformation in the zone between 50°S and 55°S.

MACQUARIE–ANTARCTIC AND MACQUARIE–AUSTRALIA ROTATIONS

The most direct way to calculate Macquarie–Australia motion is to calculate Macquarie–Antarctic motion (i.e. motion on the SEIR east of the Tasman FZ) and then sum it with Antarctic–Australia motion. Ideally, we would use the Hellinger method to calculate Macquarie–Antarctic rotations for the same anomalies in the region between the Tasman FZ and the MTJ as we did for the main part of the SEIR. However, the very limited region for which magnetic data are available (essentially there are only useful magnetic anomaly points east of the Balleny FZ) and the limited constraints on the fracture zone crossings, make it very difficult to constrain Macquarie–Antarctic rotations for most anomalies. We were able to obtain a good solution using the Hellinger method for anomaly 2Ay because it has exceptionally good magnetic anomaly coverage (Fig. 4) and we were also able to obtain a solution for anomaly 3Ay, although the data coverage was poorer and the uncertainty ellipse was considerably larger. The rotation parameters and covariance matrices for these rotations are given in Tables 3 and 4, respectively.

The location of the best-fit chron 2Ay and 3Ay Macquarie–Antarctic poles and their 95 per cent confidence zones are shown in Fig. 8. The best-fit poles are located near the southwest end of the confidence zone for the Conder & Forsyth (2000) '1 Ma' rotation. The more northeasterly position of the Conder & Forsyth (2000) pole may be driven by the azimuths and focal mechanism solutions of the transforms between 148°E and 140°E, which are representative of the instantaneous motion but not necessarily of the motion east of the Tasman FZ averaged over the last several Myr.

Using the Macquarie–Antarctic rotations, we calculated synthetic flowlines for the Balleny and Tasman FZs between anomaly 3Ay and the ridge (Fig. 9). As expected, the synthetic flowlines (heavy lines, filled circles) follow the observed fracture zone trends near the ridge much better than the flowlines based on the Australia–Antarctic rotations (light lines, open circles). It is significant that the predicted Macquarie–Antarctic flowline azimuth is nearly identical with the Australia–Antarctic azimuth west of roughly 145°E, indicating that the western limit of the deformation cannot be determined from the fracture zone azimuths alone.

We determined chron 2Ay and 3Ay rotation parameters for Macquarie–Australia by summing the Australia–Antarctic and Macquarie–Antarctic rotations for these anomalies. The rotation parameters and covariance matrices are given in Tables 3 and 4, respectively. The best-fit rotation poles and the uncertainty ellipses associated with them are shown in Fig. 8. The uncertainty ellipses of both rotations intersect the intraplate seismicity zone in the South Tasman Sea, and both of the best-fit poles fall within the seismicity zone: the Chron 2Ay pole lies near the south central edge of the seismicity zone and the Chron 3Ay pole lies near the western edge. If we assume that the intraplate seismicity outlines a zone of diffuse deformation, then the situation is similar to that found for the rotations defining Capricorn–Australia, Capricorn–India and India–Australia motion. In all of those cases the Euler pole lies in the deformation zone separating the rigid plates (Royer & Gordon 1997; Gordon 1998; Zatman *et al.* 2001).

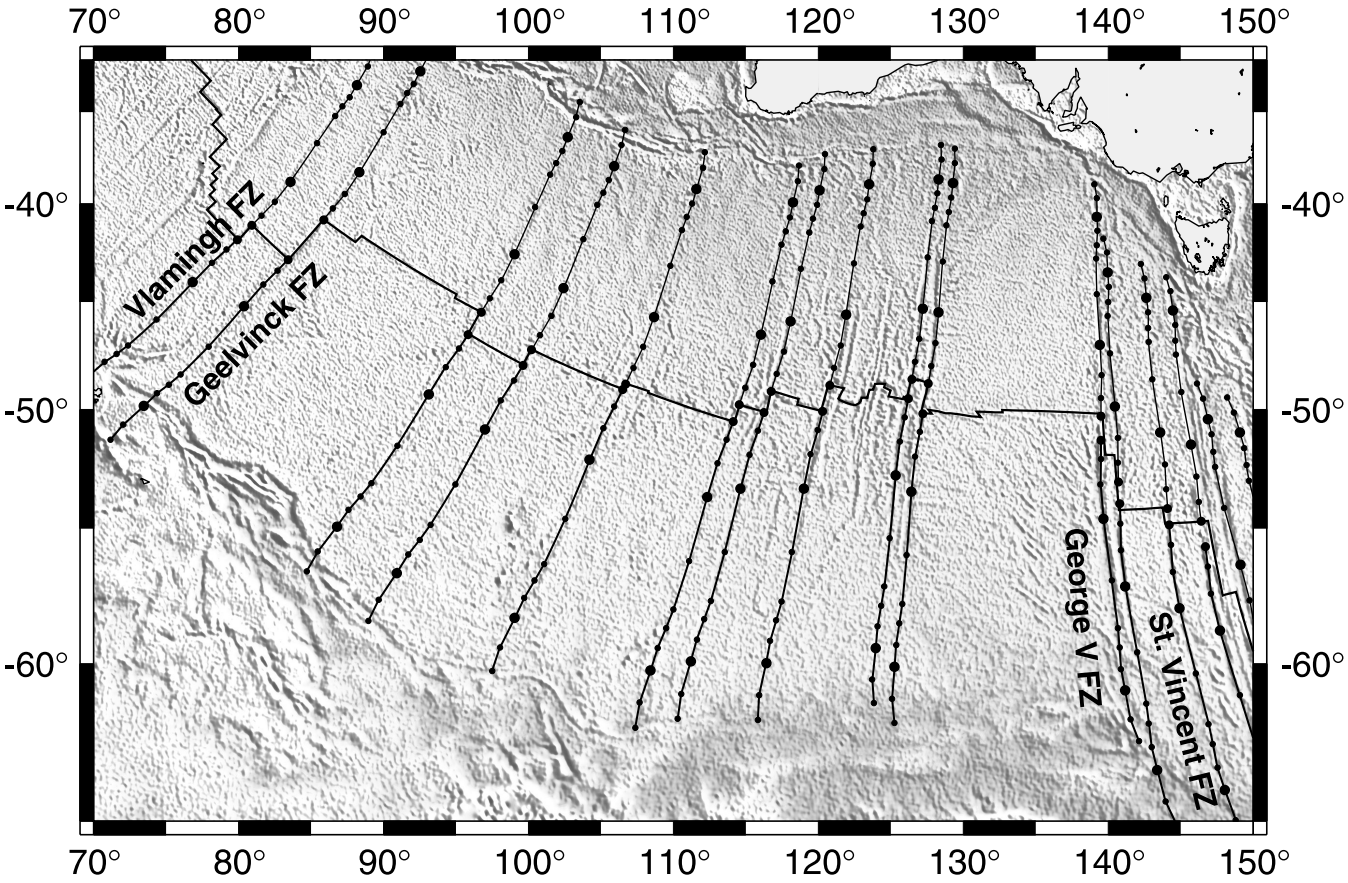

Figure 6. Comparison of synthetic flowlines with observed fracture zones on the SEIR. The filled circles mark the position of the flowline at anomalies 2Ay, 3Ay, 5o, 6o, 8o, 10o, 12o, 13o, 17o and 20o, going away from the ridge, respectively. For clarity, points corresponding to anomalies 5o and 13o are enlarged. Note that the synthetic flowlines match the trends of all of the fracture zones between 80°E and 145°E. The flowlines are shown superimposed on the satellite-derived gravity field of Sandwell & Smith (1997).

MOTION PREDICTED BY MACQUARIE–AUSTRALIA ROTATIONS

The validity of the Macquarie–Australia rotations can be checked by examining how well they predict the motion of features on the Macquarie Plate. As we noted earlier, in order to match the fracture zones on the older parts of the Antarctic and Australian plates with synthetic flowlines based on Australia–Antarctic rotations, the flowlines have to be generated from points offset from the ridge-transform intersections. If the region has behaved as a rigid plate, the Macquarie–Australia rotation for Chron 3Ay should rotate these offset synthetic flowlines back to the observed position of the Balleny and Tasman FZs. In Fig. 10 we perform this test by rotating the offset synthetic flowlines north of the SEIR by the Chron 3Ay rotation. The rotated points fall exactly on top of the observed gravity lows marking the Balleny and Tasman FZs. As part of this analysis we show the error ellipses corresponding to the Chron 3Ay rotation and we also show the amount that the points are rotated by the Chron 2Ay rotation. The effect of the Chron 2Ay rotation is much smaller than the 3Ay rotation, both because the angle is less and because the pole is located farther south and closer to the points being rotated.

As an additional check on the rotations, we also rotated magnetic anomaly points that were first rotated from the Antarctic Plate back to the Australian Plate. As we noted in Fig. 4, the magnetic anomaly points rotated from the Antarctic Plate appear to overlie their Australia counterparts although they are offset to the northeast. To test the Macquarie Plate rotations, we calculated trajectories for a few selected points for each anomaly isochron (i.e. anomalies 3Ay, 5o, 6o and 8o) using the chron 2Ay and 3Ay Macquarie–Australia rotations. These trajectories are shown by the solid lines and filled triangles in Fig. 10, with accompanying uncertainty ellipses on the position of the rotated points. It is apparent from Fig. 10 that in general the rotations reduce the along isochron misfit in the rotated Antarctic Plate anomalies that we observed in Fig. 4. However, the Chron 3Ay Macquarie–Australia rotation introduces a small across-isochron misfit, although given the large size of the uncertainty ellipses this misfit may not be significant. This across-isochron misfit, which is greatest on the eastern end of the older isochrons (i.e. anomalies 6o and 8o), suggests that the actual pole for Chron 3Ay is located further east and north than the calculated best-fit position of the pole. Because of the large offset on the Balleny FZ and the sparsity of bathymetric constraints on its structure, there may be a large systematic error in our estimate of the location of the fracture zone which is based almost entirely on the satellite-derived gravity data. Alternatively, the region that can be considered as a rigid plate may not extend this far to the north and east.

Another constraint on the motion of the Macquarie Plate comes from deformation that we have observed on archival USNS *Eltanin* single-channel seismic profiler data. In examining seismic reflection profiler data in the intraplate seismicity zone we located two single channel profiles collected on the USNS *Eltanin* in 1972 (Hayes

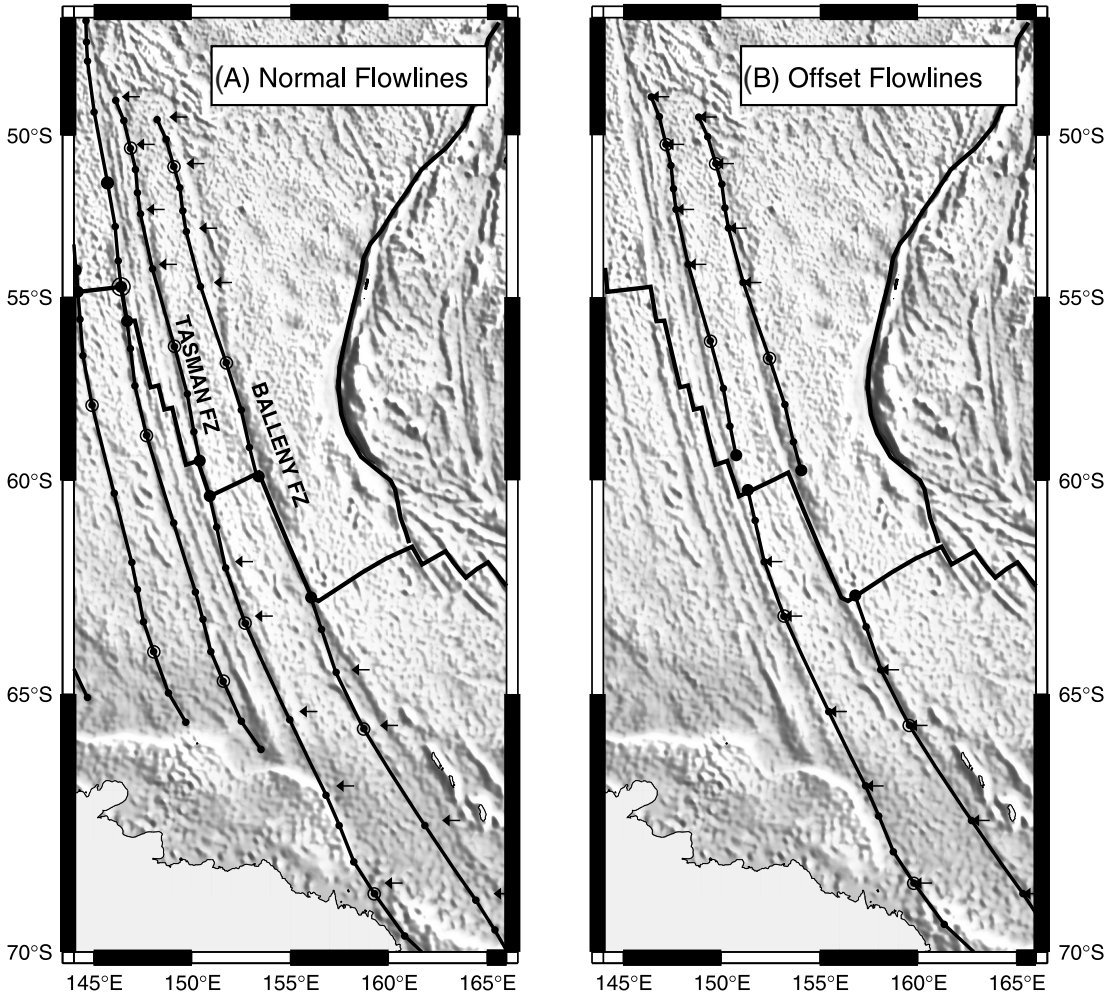

Figure 7. (A) Synthetic flowlines showing the predicted motion of the Australian and Antarctic plates in the eastern part of the SEIR. For clarity points corresponding to anomalies 5o and 13o are circled. Note that although there is a large misfit for the Tasman and Balleny FZs near the ridge, the flowlines parallel the observed fracture zones on the Antarctic Plate for anomalies 3Ay and older. Arrows show the expected position of the flowline based on the gravity data. (B) Synthetic flowlines for the Balleny and Tasman FZs generated from points offset roughly 30 km east of the points in the left frame. Note that on the Antarctic Plate the flowlines overlie the observed fracture zones for anomalies 3Ay and older, whereas on the Australian Plate the flowlines overlie the observed fracture zones only north of roughly 55°S.

Table 3. Finite rotations for the Macquarie Plate.

Plate pair (2nd plate fixed)	Chron	Lat (° N)	Long (°E)	Angle (deg)	Mag Pts	FZ Pts	Mag Segs	FZ Segs
Macquarie–Ant.	2Ay	−37.069	−162.971	2.666	13	20	1	2
Macquarie–Ant.	3Ay	−34.415	−160.704	5.562	14	21	2	2
Aus.–Macquarie	2Ay	−54.178	151.513	−1.572	NA	NA	NA	NA
Aus.–Macquarie	3Ay	−51.685	147.623	−2.954	NA	NA	NA	NA
Macquarie–Pac.	2Ay	−58.283	171.550	4.286	NA	NA	NA	NA
Macquarie–Pac.	3Ay	−58.642	171.976	9.184	NA	NA	NA	NA

NA = not applicable.

et al. 1978) that reveal a zone of compressive structures at least 50 km broad near 52°S, 148°E (Fig. 11). The style of deformation apparent in these records is similar to the compressive deformation observed in the central Indian Ocean in the diffuse plate boundary zone separating the Capricorn and Indian plates (e.g. Weissel *et al.* 1980; Bull & Scrutton 1992). Based on the topography from the two adjacent *Eltanin* lines that crossed these folds, the axis of folding appears to be roughly 75°E/255°W, parallel to the magnetic lineation direction. To the resolution of the records, the faulting appears to extend up to the seafloor. These records are consistent with a Macquarie–Australia Euler pole that is located east of 148°E. Although this is consistent with the location of the best-fit 2Ay pole, which is located at 151°E, it is not consistent with the best-fit 3Ay pole which is located almost exactly beneath the *Eltanin* lines. This could reflect the fact that the deformation occurred towards the end of the 6 Myr period, after the pole had shifted to the east, or it may

Table 4. Covariance matrices for finite rotations in Table 3.

Plate pair (2nd plate fixed)	Chron	$\hat{\kappa}$	a	b	c	d	e	f	g
Macquarie–Ant.	2Ay	15.6	1.09	−0.46	2.11	0.20	−0.90	4.10	4
Macquarie–Ant.	3Ay	4.22	2.34	−1.10	4.22	0.52	−1.98	7.61	4
Aus.–Macquarie	2Ay	6.45	1.17	−0.53	2.16	0.24	−0.96	3.99	4
Aus.–Macquarie	3Ay	2.41	2.40	−1.10	4.26	0.51	−1.94	7.59	4
Macquarie–Pac.	2Ay	5.59	1.16	−0.52	2.15	0.24	−0.97	3.99	4
Macquarie–Pac.	3Ay	4.54	2.34	−1.10	4.22	0.52	−1.98	7.62	4

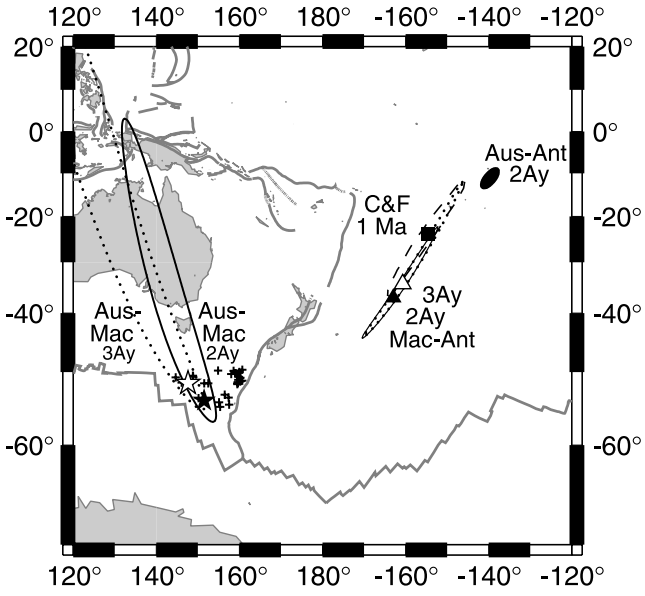

Figure 8. Location of the Macquarie–Antarctic (triangles) and Macquarie–Australia (stars) rotation poles. The Macquarie–Antarctic poles are constrained by data between the Tasman FZ and Macquarie Triple Junction. The Chron 2Ay best-fit poles and uncertainty ellipses are shown by filled symbols and solid lines respectively, while the Chron 3Ay best-fit poles and uncertainty ellipses are shown by open symbols and dotted lines respectively. The filled square marked C&F/1Ma indicates the best-fit pole and uncertainty ellipse for the 1 Ma pole of Conder and Forsyth (2000). The small filled ellipse marked Aus-Ant/2Ay shows the 95 per cent confidence zone associated with the Australia–Antarctic rotation.

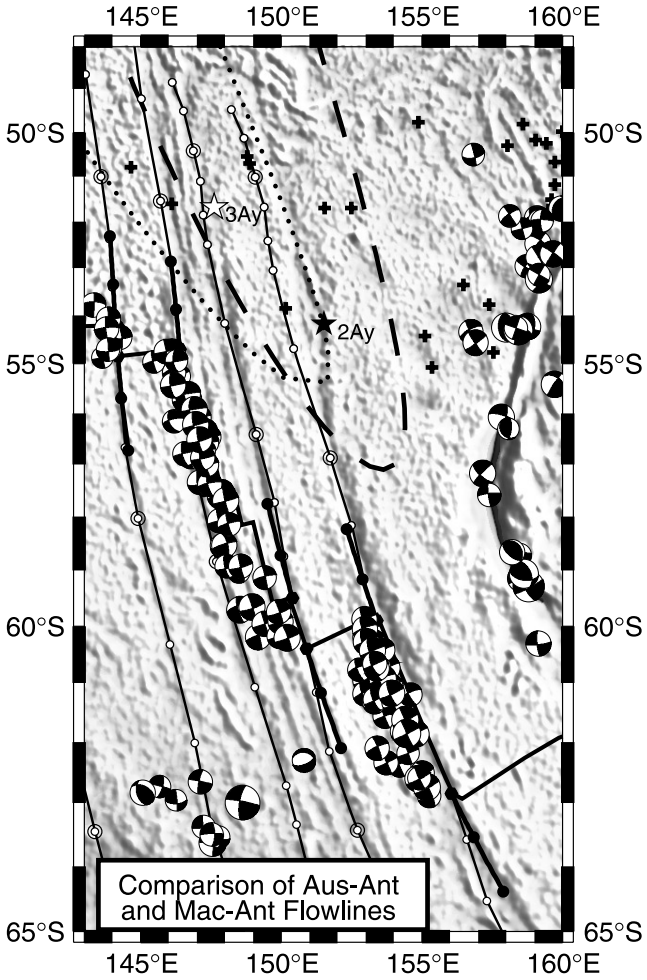

Figure 9. Synthetic flowlines for anomalies 2Ay and 3Ay predicted by the Macquarie–Antarctic rotations (filled circles, heavy solid lines). Note that these flowlines match the observed trend of the young sections of Balleny and Tasman FZs much better than the synthetic flowlines based on the Australia–Antarctic rotations (light lines, open symbols). Also shown are the locations of the best-fit Macquarie–Australia poles for 2Ay (filled star) and 3Ay (open star) and the locations of the intraplate earthquake epicentres from Valenzuela & Wysession (1993) (plusses). The focal mechanisms are centroid-moment tensor solutions from the Harvard Catalog for earthquakes with $M_b > 4.0$ at depths < 100 km between 1977 and 2003. The dashed and dotted ellipses show the 95 per cent confidence ellipses associated with the 2Ay and 3Ay Macquarie–Australia rotations, respectively.

indicate that the 3Ay pole was actually located east of the best-fit location.

Earthquake focal mechanisms in the eastern part of the intraplate seismicity zone are in agreement with the location of the 2Ay and 3Ay poles. Centroid-moment tensor solutions (Dziewonski & Woodhouse 1983) from the Harvard Catalog are shown in Fig. 9. The focal mechanisms are best resolved near the Macquarie Ridge (e.g. Das 1993; Valenzuela & Wysession 1993). In the region just west of the great 1989 Macquarie Ridge quake (52°S, 160°E) the intraplate earthquakes generally have roughly horizontal, approximately north–south, T-axes, consistent with a north–south extension direction inferred to exist between the Australian and Macquarie plates here.

A larger question is whether there is evidence in the South Tasman Sea for sufficient deformation to be consistent with the amount predicted by the 3Ay rotation. The best-fit Chron 3Ay rotation predicts roughly 60 km of north–south extension in the eastern part of the intraplate seismicity zone, near the Macquarie Ridge, although it predicts essentially no deformation near the Tasman FZ, where the pole is located. If the total motion over the last 6 Myr is more accurately modelled by a pole near the centre of the intraplate seismicity zone, say near 153°E, then there should be roughly 30 km of north–south extension near the Macquarie Ridge and about 30 km of compression near the Tasman FZ. West of the Tasman FZ the amount of predicted north–south compression increases and by the George V FZ at 140°E there is a prediction of about 50 km of north–south compression.

There are insufficient seismic reflection profiles in this region to independently constrain the amount and location of diffuse deformation that might have occurred. Although the *Eltanin* 53 profiles indicate that there has been some compressive deformation in the region, these data do not constrain the extent of the deformation zone. However, even without adequate seismic reflection data, we can set some limits on the area where deformation may have occurred. Specifically, it seems very unlikely that there is any substantial

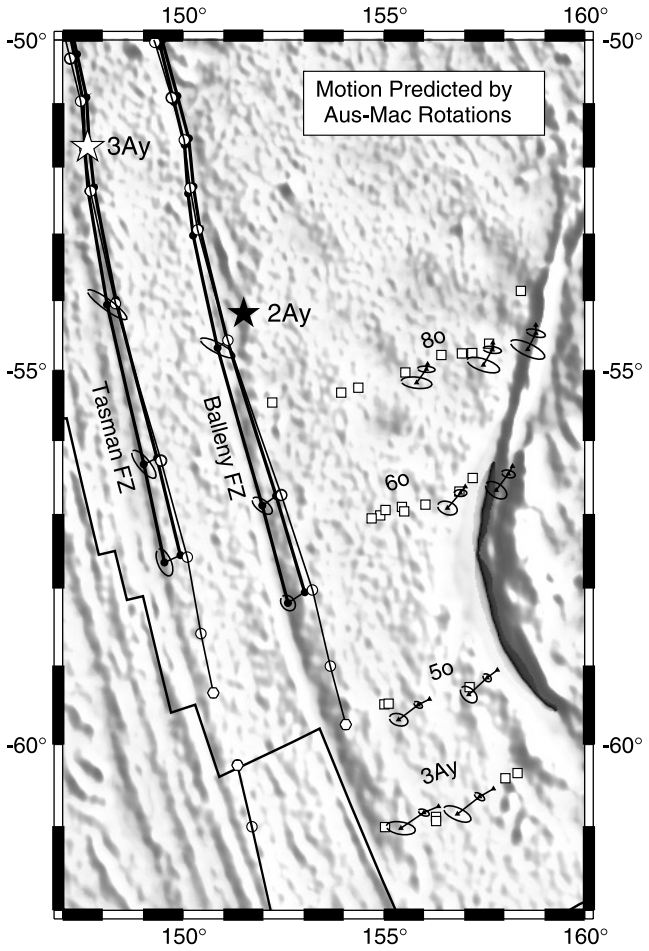

Figure 10. Demonstration of how the Macquarie–Australia rotation since Chron 3Ay causes the misfit of the Tasman and Balleny FZs. Dark lines with filled circles show the result of rotating the offset synthetic flowlines for the Balleny and Tasman FZs (shown in Fig. 7B) about the 2Ay and 3Ay rotation poles of Australia with respect to the Macquarie Plate. After the synthetic flowlines are rotated about the anomaly 3Ay pole they overlie the observed position of the fracture zones. Uncertainty ellipses are included for the fracture zone points rotated by the 3Ay rotation. Also shown are Australian Plate anomalies 3Ay to 8o east of the Balleny FZ (open symbols) and the trajectories of a few selected Antarctic anomalies rotated first about an Australia–Antarctic pole and then about the Macquarie–Australia 2Ay and 3Ay poles (filled triangles). Uncertainty ellipses are shown for the Macquarie–Australia 2Ay and 3Ay rotations. Note that the rotated anomalies along the eastern end of the anomaly 8o and 6o isochrons tend to have an across-isochron misfit. This misfit suggests that the actual 3Ay pole may be east of the best-fit pole position.

amount of deformation west of the Tasman FZ. The predicted plate motion north of the SEIR between the Tasman FZ and the George V FZ is quite large (30 to 50 km) and yet, as Fig. 4 shows, there are no observable magnetic anomaly misfits in the rotated anomaly data. Hence, we believe the deformation zone terminates at the Tasman FZ, perhaps by strike-slip motion along the old splays of the fracture zone connecting south to the ridge axis. There is little evidence to judge whether there has been 30 or 40 km of north–south extension in the eastern part of the deformation zone. Much of this area was generated during slow spreading in the Early Cenozoic, and is characterized by rough basement topography. We have not observed signs of recent extensional faulting in the crust on the few seismic profiles in this region although broadly distributed extensional deformation is likely to be difficult to recognize.

Deformation of the Macquarie Plate region has a potential impact on the calculation of Cenozoic motion between East and West Antarctica. Cande *et al.* (2000) constrained the motion between East and West Antarctica in part by analysing the misfit of anomalies on the Australian Plate east of the Balleny FZ after being rotated back to Antarctica by Australia–Antarctic rotations. They found that there was a misfit starting with a small ∼10 km misfit for anomaly 10 and increasing to a large ∼180 km misfit for anomaly 20. Since the spreading corridor east of the Balleny FZ abuts against the Iselin Bank and West Antarctica, this misfit is consistent with the separation of East and West Antarctica between chrons 20 and 10. This motion is independently constrained by magnetic anomalies flanking the Adare Trough in the northern Ross Sea. If the deformation of the Macquarie Plate involved the South Tasman Sea crust in the region of the anomalies on the Australian Plate used by Cande *et al.* (2000), this motion would affect the calculation of East–West Antarctic motion. However, for several reasons the effect is likely to have been small. First, the region on the Australian Plate involved in the estimation of East–West Antarctic motion (the area of anomalies 10 to 20) is the zone east of the Balleny FZ between 50°S and 55°S. This region is likely to be close to the pole of Macquarie–Australia rotation and, hence, least affected by the rotation. Second, the amount of the misfit attributable to East–West Antarctic motion ranges from 75 km at anomaly 13o to 180 km for anomaly 20o. These misfits are much greater than the misfits that can be attributed to Macquarie–Australia rotations in this region. Third, the sense of the across isochron misfit that is caused by the Australia–Macquarie rotation is opposite to that attributable to East–West Antarctic motion. That is, to the extent that an Australia–Macquarie rotation about the best-fit 3Ay pole caused an across-isochron misfit, this misfit would decrease the apparent spreading rate east of the Balleny FZ whereas the observed East–West Antarctic motion acted to increase the apparent spreading rate east of the Balleny FZ. Thus, the Macquarie–Australia rotation proposed here is unlikely to cause a significant change in the estimate of the amount of Cenozoic motion between East and West Antarctica.

PACIFIC–AUSTRALIA MOTION AND SUBDUCTION AT THE HJORT TRENCH

The plate kinematic history of the Macquarie Ridge and Hjort Trench region is very unusual. Between roughly 45 Ma and 30 Ma this section of the Pacific–Australia plate boundary was an active ridge, generating the ocean crust that is now found in the Emerald Basin and in the eastern part of the Southern Tasman Sea (Weissel *et al.* 1977; Sutherland 1995). Starting about 30 Ma the motion along this boundary became progressively more strike-slip until by 20 Ma it was essentially a strike-slip boundary. Over the last 20 Myr, the relative motion along the boundary has varied and at times there has been a strong component of convergence across parts of the boundary. Weissel *et al.* (1977) showed that along the centre section of the Macquarie Ridge, near 55°S, nearly 200 km of young Australian Plate crust is missing and must have been subducted.

As a consequence of this unusual plate motion history, there are several enigmatic issues related to the tectonics of the plate boundary (e.g. Massell *et al.* 2000). For example, focal mechanisms in the Hjort Trench region are mostly strike-slip (Frohlich *et al.* 1997; Ruff *et al.* 1989) even though global plate motion models such as NUVEL1-A (DeMets *et al.* 1994) predict a convergence angle of

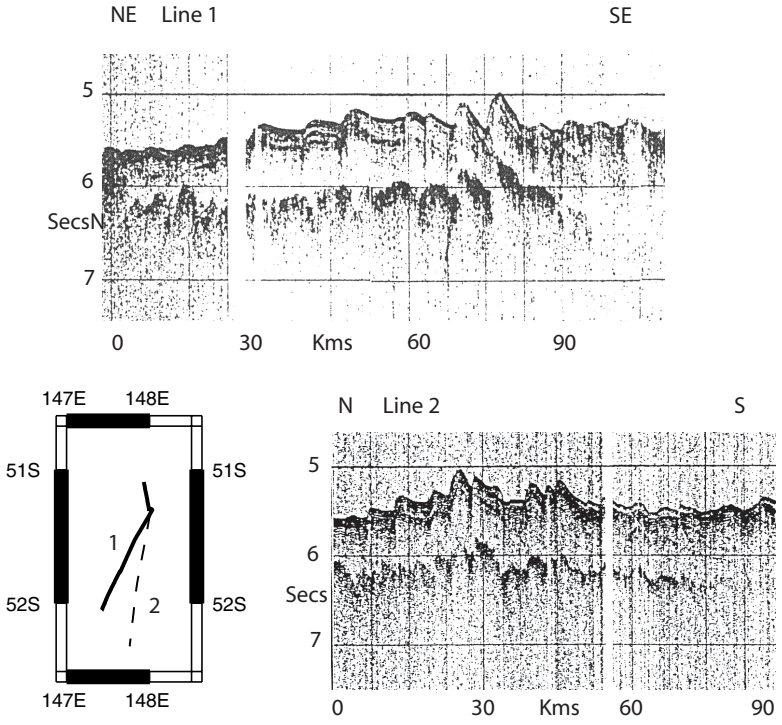

Figure 11. Single-channel seismic profilers record from USNS *Eltanin* cruise 53 showing compressive deformation on the seafloor in the zone of intraplate seismicity. The deformation is similar in appearance to that seen on profiles in the central Indian Ocean. The location of the profiles is shown by the inset map at lower left.

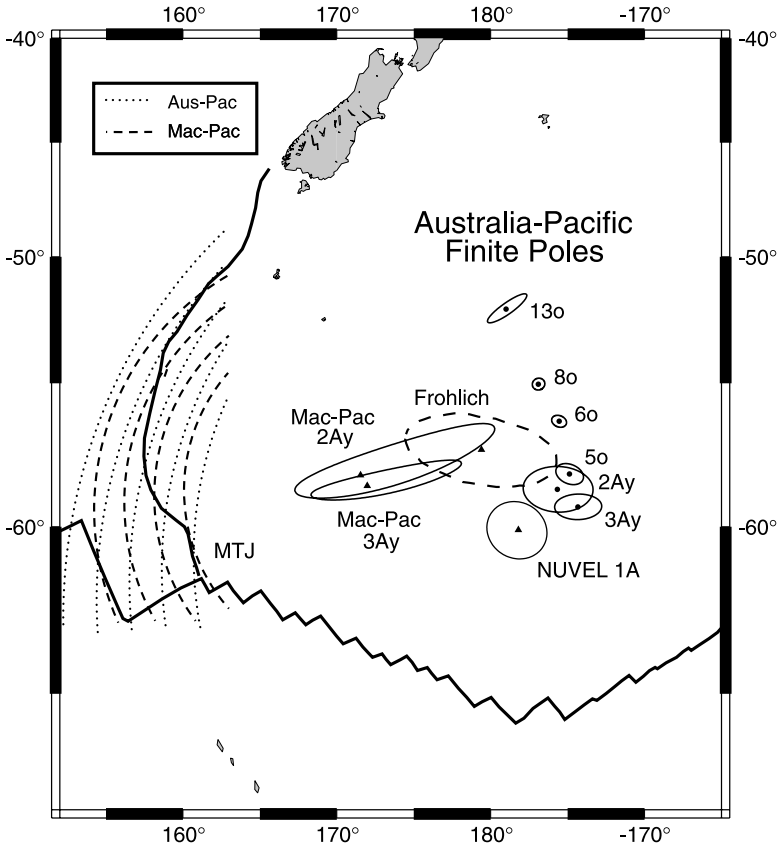

Figure 12. Location of Australia–Pacific and Macquarie–Pacific rotation poles and their 95 per cent confidence zones. The Australia–Pacific poles were determined by summing Australia–Antarctic and Pacific–Antarctic rotations going back to Chron 13o, while the Macquarie–Pacific poles were determined by summing the Macquarie–Antarctic and Pacific–Antarctic rotations for Chrons 2Ay and 3Ay. Dashed and dotted lines near the Macquarie ridge are small circles about the Macquarie–Pacific (Mac-Pac) and the Australia–Pacific (Aus-Pac) Chron 2Ay poles, respectively. Also shown are the pole and 95 per cent confidence zone based on Macquarie Ridge focal mechanisms (Frohlich *et al.* 1997) and the NUVEL-1A Pacific–Australia pole (DeMets *et al.* 1994).

Table 5. Finite rotations of Antarctica relative to the Pacific.

Chron	Lat (° N)	Long (°E)	Angle (deg)	Mag Pts	FZ Pts	Mag Segs	FZ Segs
2Ay	65.532	−79.484	−2.259	41	11	4	1
3Ay	66.988	−81.949	−5.195	39	13	5	1
5o	70.335	−77.855	−9.479	35	10	5	1
6o	74.202	−69.520	−16.870	20	11	4	1
8o	74.773	−66.940	−21.826	17	40	4	4
13o	74.399	−64.556	−27.360	30	31	7	5

Rotations are from Cande & Stock (in preparation).

Table 6. Covariance matrices for finite rotations in Table 5.

Chron	$\hat{\kappa}$	a	b	c	d	e	f	g
2Ay	4.01	7.14	−0.107	8.08	1.59	3.17	20.5	8
3Ay	4.77	10.5	1.09	11.3	4.90	7.98	29.3	8
5o	2.89	1.63	−0.238	1.44	1.11	1.50	4.92	7
6o	.65	8.48	−0.107	7.74	5.03	8.89	29.5	8
8o	.75	4.37	1.74	12.0	1.49	5.28	37.6	7
13o	1.59	7.00	5.97	12.0	5.98	10.8	24.8	7

roughly 20° near 58°S increasing to about 50° at the south end of the Hjort Trench. Frohlich *et al.* (1997) determined a Pacific–Australia Euler pole based solely on focal mechanisms from the Macquarie Ridge and Hjort Trench and found that it was located north and west of the NUVEL-1A pole (Fig. 12) and predicted less convergence. With our estimate of a Macquarie–Antarctic rotation we can now independently estimate the motion across the Macquarie Ridge and Hjort Trench for the last 6 Myr by summing the motion of Macquarie–Antarctic and Antarctic–Pacific.

Our new Australia–Antarctic rotations were combined with Pacific–Antarctic rotations for chrons 2Ay, 3Ay, 5o, 6o, 8o and 13o in order to calculate Pacific–Australia rotations. The Pacific–Antarctic rotations are from Cande & Stock (in preparation) and were determined using the Hellinger method (Tables 5 and 6). The constraints used to calculate the Pacific–Antarctic rotations include data collected on the R/VIB *Nathaniel B. Palmer* in the last few years and the solutions are preferred to those published by Cande *et al.* (1995). Rotation parameters and covariance matrices for Pacific–Australia motion for chrons 2Ay to 13o are given in Tables 7 and 8. The Chron 13o Australia–Antarctic rotation parameters are from Cande *et al.* (2000) and include the effects of East–West Antarctic motion (Tables 9 and 10). The Pacific–Australia Euler poles and their uncertainty ellipses are shown in Fig. 12.

We determined Pacific–Macquarie rotations for chrons 2Ay and 3Ay by summing the Macquarie–Antarctic rotations with our estimates of the Chron 2Ay and 3Ay Antarctic–Pacific rotations (Tables 3 and 4). The Pacific–Macquarie 2Ay and 3Ay best-fit poles lie closer to the Macquarie Ridge and Hjort Trench than do our revised Pacific–Australia poles, the NUVEL1-A pole or even the

Table 7. Finite rotations of Australia relative to the Pacific.

Chron	Lat (° N)	Long (°E)	Angle (deg)
2Ay	−58.761	−175.666	2.766
3Ay	−59.347	−174.331	6.385
5o	−58.244	−174.873	11.933
6o	−56.392	−175.556	22.217
8o	−55.030	−176.889	29.232
13o	−52.142	−178.990	37.107

Table 8. Covariance matrices for finite rotations in Table 7.

Chron	$\hat{\kappa}$	a	b	c	d	e	f	g
2Ay	4.76	3.55	−3.37	3.43	5.29	− 4.59	11.1	7
3Ay	2.60	4.09	−3.81	4.40	6.68	−5.14	11.9	7
5o	1.22	3.21	−1.98	2.17	3.90	−0.692	9.42	7
6o	0.97	2.66	−1.90	1.24	3.27	−1.09	7.20	7
8o	.91	10.5	−3.12	17.0	4.53	−4.16	39.9	7
13o	.73	5.18	−1.98	7.72	0.86	−2.94	11.6	5

Table 9. Finite rotation of Australia relative to West Antarctica.

Chron	Lat (° N)	Long (°E)	Angle (deg)
13o	−12.600	−147.298	20.848

Rotation is from Cande *et al.* (2000).

pole of Frohlich *et al.* (1997) (Fig. 12). As a consequence, our Pacific–Macquarie poles predict motion near the Hjort Trench that is more parallel to the trench than would be expected using the Pacific–Australia Euler poles. To demonstrate this, in Fig. 12 we have drawn small circles about both the Pacific–Macquarie Chron 2Ay pole (dashed lines) and our Pacific–Australia Chron 2Ay pole (dotted lines). Thus, the more westerly location of the Pacific–Macquarie poles may help to explain, in part, the prevalence of strike-slip faulting observed along the Hjort Trench. However, the apparent prevalence of strike-slip mechanisms can also be attributed to strain-partitioning in which the strike-slip mechanisms are found along the crest of the ridge and thrust mechanisms along the trench axis (Meckel *et al.* 2003).

The predicted Pacific–Macquarie motion since Chron 3Ay near the MTJ also agrees better with recent swathmap observations of the transform fault connecting the MTJ to the Hjort Trench (Bernardel & Symonds 2001) than predictions based on the Pacific–Australia rotations. The swathmap data of Bernardel & Symonds (2001) show that this transform has a strike of N25°W near 61°S. The Pacific–Australia rotation predicts a nearly north–south transform azimuth at this latitude while our Pacific–Macquarie Chron 2Ay rotation predicts an azimuth of N18°W.

The difference in the net displacement since Chron 3Ay predicted by Pacific–Australia and Pacific–Macquarie rotations is dramatic and suggests a cause for the onset of deformation of the Australian Plate in the South Tasman Sea, forming the Macquarie Plate, at 6 Ma. We calculated trajectories for several points on the Australian Plate relative to the Macquarie Ridge and Hjort Trench, using both the Pacific–Australia rotations and the Pacific–Macquarie rotations (Fig. 13). In the central portion of the Macquarie Ridge the predicted plate motion direction is nearly the same for both sets of rotations. However, across the southern Hjort Trench, the predicted motion differs, with the Pacific–Australia rotations resulting in an increasing angle of convergence in Late Miocene time. At both chrons 5o and 3Ay, the predicted Pacific–Australia convergence direction rotates clockwise becoming increasingly perpendicular to the trench, although the rate of displacement remains fairly constant. However, with the Pacific–Macquarie trajectories there is essentially no change in direction at Chron 3Ay while there is a roughly 35 per cent

Table 10. Covariance matrix for rotation in Table 9.

Chron	$\hat{\kappa}$	a	b	c	d	e	f	g
13o	.63	5.06	−2.02	7.56	0.84	−2.99	11.4	5

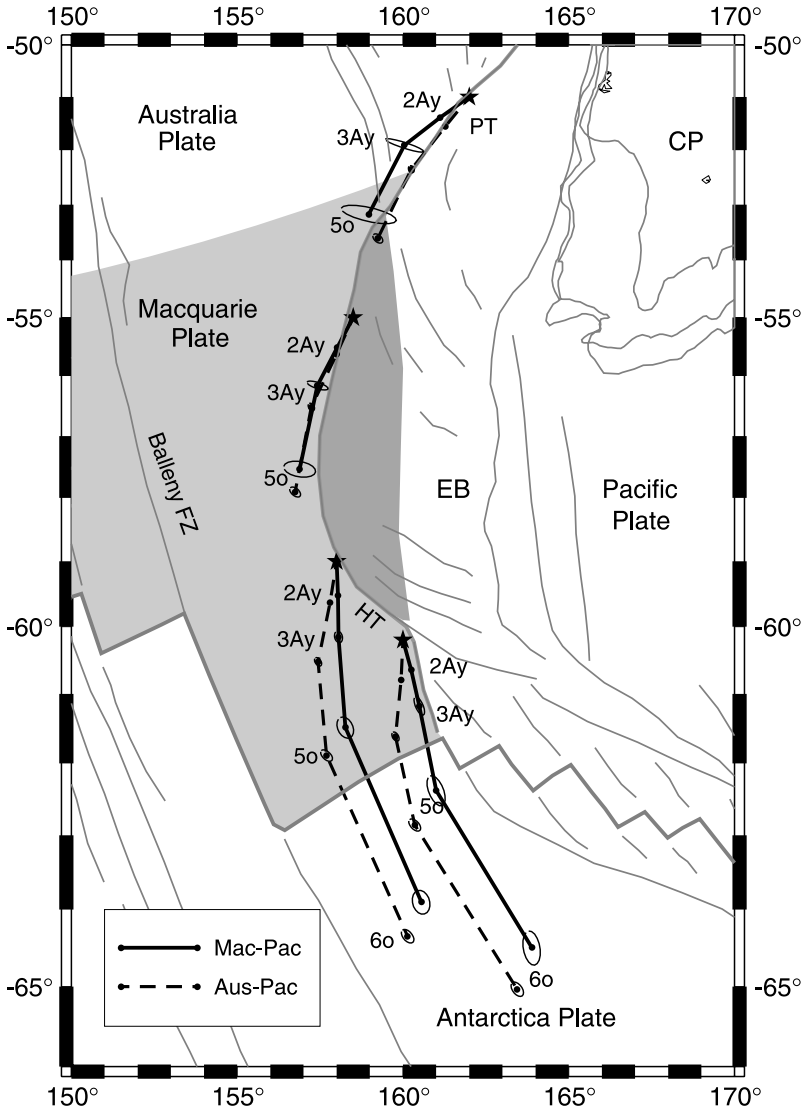

Figure 13. Predicted plate motion trajectories for the Australian Plate relative to the Pacific Plate (dashed lines) and the Macquarie Plate relative to the Pacific Plate (solid line) for chrons 2Ay, 3Ay, 5o and 6o for several points along the Macquarie Ridge and Hjort Trench (HT). Note that the Australia–Pacific motion near the Hjort Trench has a clockwise kink at 3Ay, while the Macquarie–Pacific motion slows down and does not change direction. For clarity, the Chron 6o points are only shown on the two southernmost trajectories. The light shaded region marks the Macquarie Plate; the dark shaded region marks extent of the Australia (Macquarie) Plate subducted beneath the Macquarie Ridge. PT = Puyseguer Trench, CP = Campbell Plateau, EB = Emerald Basin.

decrease in the rate of displacement (from 28 mm yr^{-1} to 18 mm yr^{-1}). In addition, the convergence rate orthogonal to the southern Hjort Trench calculated with the Pacific–Macquarie rotations is roughly half that predicted from the Pacific–Australia rotations between Chron 3Ay and the present.

The onset of deformation in the South Tasman Sea and the development of an independent Macquarie Plate may have been triggered by the buoyancy of young oceanic crust entering the southern Hjort Trench. With the gradual change in the Pacific–Australia motion in Late Miocene time at the latitude of the Hjort Trench, the convergence direction was becoming more perpendicular to the trench, causing greater subduction of young buoyant crust. Around Chron 3Ay, a threshold level appears to have been crossed, coinciding with a clockwise change in Pacific–Australia motion, in which it became easier for the Australian Plate to deform in the region of 50°S to 55°S in the South Tasman Sea than it was for the plate to subduct a greater amount of young oceanic crust in the southern Hjort Trench. However, it is not clear to what extent the change in Pacific–Australia motion triggered this response or, alternatively, the development of the Macquarie Plate caused the change in Pacific–Australia motion.

IMPLICATIONS FOR NEW ZEALAND TECTONICS

A full discussion of the implications of the revised Pacific–Australia rotations for the tectonics of the Pacific–Australia boundary north of the Macquarie Ridge is beyond the scope of this paper. However, we will briefly point out here some important implications for the tectonics of the Alpine Fault region in New Zealand. The kinematic setting of the Alpine Fault is determined by the summation of Australia–Antarctic and Antarctic–Pacific motions and the calculation of the relative displacement vector across the Pacific–Australia boundary (Molnar *et al.* 1975; Walcott 1998). As the estimates of

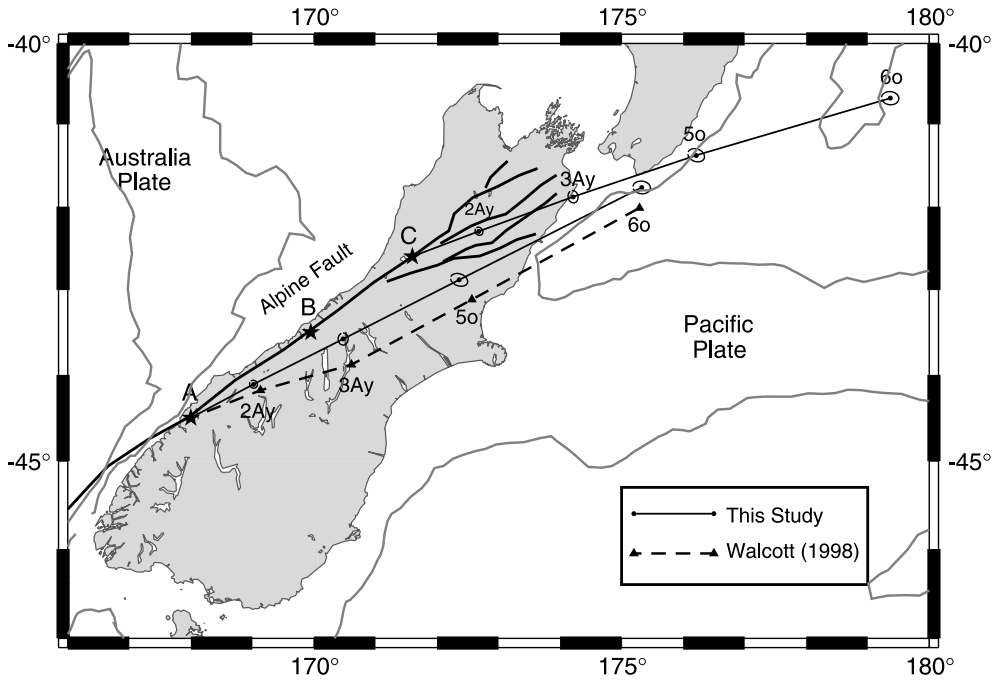

Figure 14. Predicted plate motion trajectories for the Pacific Plate relative to the Australian Plate (fixed) for two points (A & C) along the Alpine Fault. The solid lines with the uncertainty ellipses shows the trajectory based on the new Australia–Pacific rotations. The dashed line shows the trajectory based on the rotations of Walcott (1998). Note that the revised trajectories have very little change in convergence direction over the last 20 Myr.

Pacific–Antarctic and Australia–Antarctic rotations have improved over the years, the inferred displacement history has changed. For example, Walcott (1998) proposed that there was a pronounced clockwise change in convergence direction around 6 Ma. However, because there were no intermediate rotation poles for the SEIR for the period around 6 Ma, this conclusion was obtained by interpolating a 6 Ma rotation for Australia–Antarctic motion between the Royer & Sandwell (1989) Chron 5o rotation and the NUVEL-1A (DeMets *et al.* 1994) rotation.

With our new Australia–Antarctic rotations for chrons 3Ay and 2Ay, a detailed Late Miocene history can be directly calculated without interpolation of the Australia–Antarctic rotations. In Fig. 14 we show the trajectory of two points on the Pacific Plate relative to a fixed Australian Plate. We also include the error ellipses for each point. In addition, we include the trajectory based on the rotations determined by Walcott (1998). The revised trajectory has only about 60 per cent of the predicted convergence in the past 6 Myr and does not display the marked change in convergence direction at 6 Ma that was predicted by Walcott (1998). The lack of a distinct change in convergence direction at Chron 3Ay reflects the fact that we did not interpolate between a Chron 5o rotation and the NUVEL-1A pole as Walcott (1998) did.

Although the change in convergence direction at Chron 3Ay is not as pronounced as proposed by Walcott (1998), there are still some noticeable kinematic changes at that time. Fig. 15 shows the amount of displacement both perpendicular and parallel to the fault for three points along the Alpine Fault for the last 20 Myr. (These conclusions assume that all of the Pacific–Australia motion is being accommodated at the Alpine Fault and that there is no deformation elsewhere on the South Island.) At both chrons 5o and 3Ay there is an increase in the convergence rate perpendicular to the fault. The absolute increase in the rate is roughly the same at both times and at all three points; however, the percentage rate of increase is much larger at the central and southern points. In particular, at the southernmost point (at 44.5°S) there was essentially no perpendicular convergence prior to 11 Ma, whereas at the northern point (42.5°S) there was already a significant amount of convergence prior to 11 Ma. Of course, this plot only calculates the average displacement rate over the entire time interval and does not indicate when the change in rate occurred within the interval and whether it was gradual or sharp.

The lack of a major change in the convergence direction across the Alpine Fault at Chron 3Ay is intriguing. As Walcott (1998) noted, there is a significant change in Pacific–Antarctic motion at Chron 3Ay (e.g. Cande *et al.* 1995) and one might expect that there would be a major change in Pacific–Australia motion at that time. Indeed, as Fig. 13 showed, there was a significant change in the predicted Pacific–Australia motion at the latitude of the southern Hjort Trench. However, at the latitude of the Alpine Fault the change in relative motion at Chron 3Ay is much less. Apparently the changes in Pacific–Antarctic motion were compensated for by changes in Australia–Antarctic motion, with the net result that there was only a small change in the direction of Pacific–Australia motion in the New Zealand region.

SUMMARY AND CONCLUSIONS

We determined a series of nine finite rotations that describe the relative motion of the Australian and Antarctic plates over the last 40 Myr. The rotations were constrained using data on the SEIR between 88°E and 139°E, thus avoiding complexities related to the Capricorn Plate and to the enigmatic transform fault azimuths of the eastern SEIR. These rotations provide a benchmark for analysing the motion of the SEIR east of the George V FZ. Based on an analysis of the fit of fracture zone and magnetic anomalies in the eastern part of the SEIR we found the following:

(i) The region of the Australian Plate roughly east of 145°E and south of 55°S, corresponding to the Macquarie Plate of DeMets

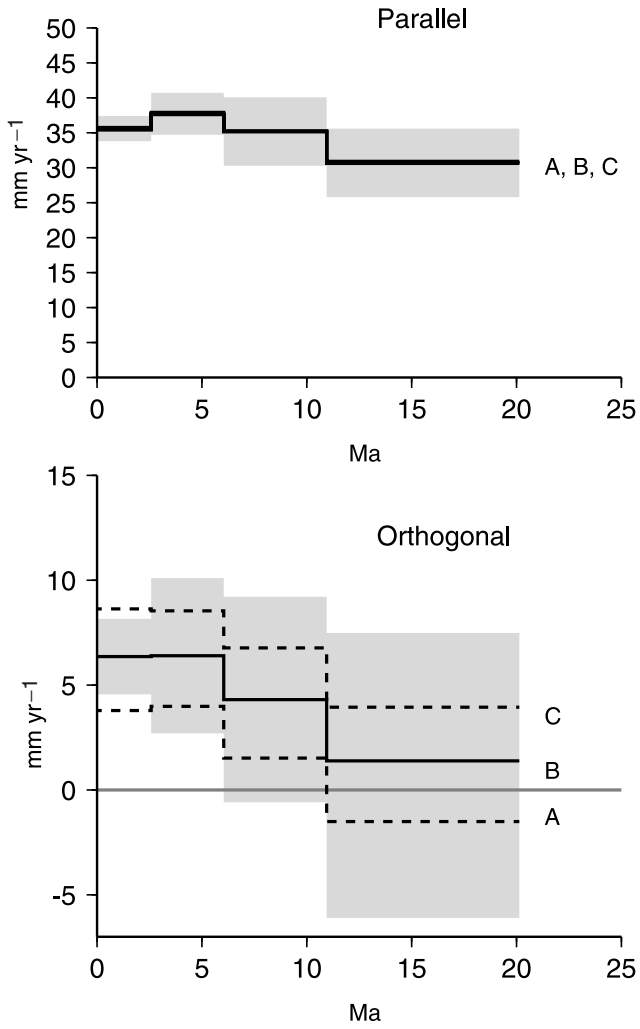

Figure 15. Relative motion of the Pacific Plate parallel (top) and orthogonal (bottom) to the Alpine Fault at points A, B and C in Fig. 14. The Australian Plate is fixed. The velocity orthogonal to the Alpine Fault increases at chrons 5o and 3Ay. The onset of convergence in the south (point A) occurs around Chron 5o. Shading shows the 95 per cent uncertainty limits on the motion of point B. The motion of points A and C are dashed for clarity.

et al. (1988), has behaved as a rigid, independent plate for the last 6 Myr.

(ii) The Macquarie Plate is separated from the main portion of the Australian Plate by a deformation zone outlined roughly by the intraplate seismicity noted by Valenzuela & Wysession (1993).

(iii) The Euler pole describing the motion of the Macquarie Plate relative to the Australian Plate is located within the deformation zone, in a fashion similar to that observed between the other component plates of the Indo-Australian Plate.

We summed Macquarie–Antarctic and Antarctic–Pacific rotations in order to calculate Pacific–Macquarie motion for the last 6 Myr. We compared this motion with Pacific–Australia motion and found the following:

(i) The Pacific–Macquarie rotations predict less convergence and a larger component of strike-slip motion across the Hjort Trench than Pacific–Australia rotations.

(ii) The onset of the deformation in the South Tasman Sea and the development of the Macquarie Plate around 6 Ma appears to have been triggered by the subduction of young, buoyant crust.

(iii) This event coincided with a clockwise change in Pacific–Australia motion at the latitude of the Hjort Trench, although it is not clear to what extent the change in plate motion triggered the deformation or, alternatively, the development of a separate Macquarie Plate contributed to the change in plate motion.

The revised Australia–Pacific rotations also have important implications for the tectonics of New Zealand. We found that:

(i) Changes in relative displacement along the Alpine Fault have been small and relatively continuous over the last 20 Myr.

(ii) The average rate of convergence (i.e. motion orthogonal to the Alpine Fault) over the last 6 Myr is about 40 per cent smaller than in previous models.

(iii) The onset of convergence along the southern Alpine Fault, near 44.5°S, occurred about 11 Ma.

ACKNOWLEDGMENTS

This study was made possible through grants from the NSF-Office of Polar Programs supporting the acquisition of underway geophysical data on long transits of the R/VIB *Nathaniel B. Palmer*. We thank the officers, crew and scientific staff of the R/VIB *Nathaniel B. Palmer* and the many graduate students and other scientists, especially Stan Jacobs, who have contributed to this programme. M. Coffin, C. DeMets and R. Gordon gave helpful reviews. GMT software was used to produce the figures (Wessel & Smith 1991). This programme was supported by NSF grants OPP-0126340 (UCSD) and OPP-0126334 (Caltech). California Institute of Technology Division of Geological and Planetary Sciences contribution number 9032.

REFERENCES

Bernardel, G. & Symonds, P., 2001. Seafloor mapping of the south-east region and adjacent waters—AUSTREA final report: southern Macquarie Ridge, *Geoscience Australia Record,*2001/46.

Bull, J.M. & Scrutton, R.A., 1992. Seismic reflection images of intraplate deformation, central Indian Ocean, and their tectonic significance, *J. geol. Soc., Lond.,* **149,** 955–966.

Cande, S.C. & Kent, D.V., 1995. Revised calibration of the geomagnetic polarity timescale for the Late Cretaceous and Cenozoic, *J. geophys. Res.,* **100,** 6093–6095.

Cande, S.C., Raymond, C.A., Stock, J.M. & Haxby, W.F., 1995. Geophysics of the Pitman Fracture Zone and Pacific-Antarctic plate motions during the Cenozoic, *Science,* **270,** 947–953.

Cande, S.C., Stock, J.M., Müller, R.D. & Ishihara, T., 2000. Cenozoic motion between East and West Antarctica, *Nature,* **404,** 145–150.

Chang, T., 1987. On the statistical properties of estimated rotations, *J. geophys. Res.,* **92,** 6319–6329.

Chang, T., 1988. Estimating the relative rotation of two tectonic plates from boundary crossings, *J. Am. Statist. Assoc.,* **83,** 1178–1183.

Conder, J.A. & Forsyth, D.W., 2000. Do the 1998 Antarctic plate earthquake and its aftershocks delineate a plate boundary?, *Geophys. Res. Lett.,* **27,** 2309–2312.

Das, S., 1992. Reactivation of an oceanic fracture by the Macquarie Ridge earthquake of 1989, *Nature,* **357,** 150–153.

Das, S., 1993. The Macquarie Ridge earthquake of 1989, *Geophys. J. Int.,* **115,** 778–798.

DeMets, C., Gordon, R.G. & Argus, D.F., 1988. Intraplate deformation and closure of the Australia-Antarctica-Africa plate circuit, *J. geophys. Res.,* **93,** 11 877–11 897.

DeMets, C., Gordon, R.G., Argus, D.F. & Stein, S., 1994. Effect of recent revisions to the geomagnetic reversal time scale on estimates of current plate motions, *Geophys. Res. Lett.,* **21,** 2191–2194.

Dziewonski, A.M. & Woodhouse, J.H., 1983. An experiment in the systematic study of global seismicity: centroid-moment tensor solutions for 201 moderate and large earthquakes of 1981, *J. geophys. Res.,* **88,** 3247–3271.

Frohlich, C., Coffin, M.F., Massell, C., Mann, P., Schuur, C.L., Davis, D., Jones, T. & Karner, G., 1997. Constraints on Macquarie ridge tectonics provided by Harvard focal mechanisms and teleseismic earthquake locations, *J. geophys. Res.,* **102,** 5029–5041.

Gordon, R.G., 1998. The plate tectonic approximation: plate nonrigidity, diffuse plate boundaries, and global plate reconstructions, *Ann. Rev. Earth planet. Sci.,* **26,** 615–642.

Gordon, R.G., 2000. Diffuse oceanic plate boundaries: strain rates, vertically averaged rheology, and comparisons with narrow plate boundaries and stable plate interiors, in The History and Dynamics of Global Plate Motions, American Geophysical Union Geophysical Monograph **121**, pp. 143–160, eds Richards, M.A., Gordon, R.G., & van der Hilst, R., American Geophysical Union, Washington, DC..

Hayes, D.E., Weissel., J., Aitken, T., Houz, R., Talwani, M., Shearer, R.A. & Watts, A.B., 1978. Preliminary Report of Volume 26, U.S.N.S. Eltanin, Cruises 51-55A, January 1972–December 1972, in *Lamont-Doherty Survey of the World*, Technical Report No. CU-1-78, ed. Talwani, M., Lamont-Doherty Geological Observatory of Columbia University, Palisades, NY.

Hellinger, S.J., 1981. The uncertainties of finite rotations in plate tectonics, *J. geophys. Res.,* **86,** 9312–9318.

Henry, C., Das, S. & Woodhouse, J.H., 2000. The great March 25, 1998 Antarctic plate earthquake: moment tensor and rupture history, *J. geophys. Res.,* **105,** 16 097–16 118.

Krijgsman, W., Hilgen, F.J., Raffi, I., Sierro, F.J. & Wilson, D.S., 1999. Chronology, causes and progression of the Messinian salinity crisis, *Nature,* **400,** 652–655.

Kubo, A., Nogi, Y. & Kaminuma, K., 1998. Systematic deviations of earthquake slip vectors from NUVEL1 at the Australia-Antarctica and Pacific-Antarctica plate boundaries, *Polar Geosci.,* **11,** 61–75.

Marks, K.M., Stock, J.M. & Quinn, K.J., 1999. Evolution of the Australian-Antarctica discordance since Miocene time, *J. geophys. Res.,* **104,** 4967–4981.

Massell, C. *et al.,* 2000. Neotectonics of the Macquarie Ridge Complex, Australia-Pacific plate boundary, *J. geophys. Res.,* **105,** 13 457–13 480.

Meckel, T.A., Coffin, M.F., Mosher, S., Symonds, P., Bernardel, G. & Mann, P., Underthrusting at the Hjort Trench, Australia-Pacific plate boundary: incipient subduction?, *Geochem. Geophys. Geosyst.*, **4,** 12, 1099. DOI: 10.1029/2002GC000498, 06 December 2003.

Molnar, P., Atwater, T., Mammerickx, J. & Smith, S.M., 1975. Magnetic anomalies, bathymetry and the tectonic evolution of the South Pacific since the late Cretaceous, *Geophys. J. R. astr. Soc.,* **40,** 383–420.

Müller, R.D. & Roest, W.R., 1992. Fracture zones in the North Atlantic from combined Geosat and Seasat data, *J. geophys. Res.,* **97,** 3337–3350.

Nettles, M., Wallace, T.C. & Beck, S.L., 1999. The March 25, 1998 Antarctic plate earthquake, *Geophys. Res. Lett.,* **26,** 2097–2100.

Royer, J.-Y. & Chang, T., 1991. Evidence for relative motions between the Indian and Australian plates during the last 20 Myr from plate tectonic reconstructions: implications for the deformation of the Indo-Australian plate, *J. geophys. Res.,* **96,** 11 779–11 802.

Royer, J.-Y. & Gordon, R.G., 1997. The motion and boundary between the Capricorn and Australian plates, *Science,* **277,** 1268–1274.

Royer, J.-Y. & Sandwell, D.T., 1989. Evolution of the Indian Ocean since the Late Cretaceous: constraints from Geosat altimetry, *J. geophys. Res.,* **94,** 13 755–13 782.

Ruff, L.J., Given, J.W., Sanders, C.O. & Sperber, C.M., 1989. Large earthquakes in the Macquarie ridge complex: transitional tectonics and subduction initiation, *Pageoph,* **129,** 71–129.

Sandwell, D.T. & Schubert, G., 1982. Lithospheric flexure at fracture zones, *J. geophys. Res.,* **87,** 4657–4667.

Sandwell, D.T. & Smith, W., 1997. Marine gravity-anomaly from Geosat and ERS-1 satellite altimetry, *J. geophys. Res.,* **102,** 10 039–10 054.

Sclater, J.G., Munschy, M., Fisher, R.L., Weatherall, P., Cande, S.C., Patriat, P., Bergh, H. & Schlich, R., 1997. *Geophysical Synthesis of the Indian/Southern Oceans: Part 1, The Southwest Indian Ocean*, SIO Reference Series No. 97-6. University of California, San Diego.

Sutherland, R., 1995. The Australia-Pacific boundary and Cenozoic plate motions in the SW Pacific: some constraints from Geosat data, *Tectonics,* **14,** 819–831.

Tikku, A. & Cande, S.C., 1999. The oldest magnetic anomalies in the Australian-Antarctic basin: are they isochrons?, *J. geophys. Res.,* **104,** 661–677.

Valenzuela, R.W. & Wysession, M.E., 1993. Intraplate earthquakes in the southwest Pacific ocean basin and the seismotectonics of the southern Tasman Sea, *Geophys. Res. Lett.,* **20,** 2467–2470.

Walcott, R.I., 1998. Modes of oblique compression: late Cenozoic tectonics of the South Island of New Zealand, *Rev. Geophys.,* **36,** 1–26.

Wiens, D.A. *et al.,* 1985. A diffuse plate boundary model for Indian Ocean tectonics, *Geophys. Res. Lett.,* **12,** 429–432.

Weissel, J.K. & Hayes, D.E., 1972. Magnetic anomalies in the Southeast Indian Ocean, in *Antarctic Oceanology II: the Australian-New Zealand Sector*, Antarctic Research Series 19, pp. 165–196, ed. Hayes, D.E., American Geophysical Union, Washington, DC.

Weissel, J.K., Hayes, D.E. & Herron, E.M., 1977. Plate tectonics synthesis: the displacements between Australia, New Zealand, and Antarctica since the late Cretaceous, *Mar. Geol.,* **25,** 231–277.

Weissel, J.K., Anderson, R.N. & Geller, C.A., 1980. Deformation of the Indo-Australian plate, *Nature,* **287,** 284–291.

Wessel, P. & Smith, W.H.F., 1991. Free software helps map and display data, *EOS, Trans. Am. geophys. Un.,* **72,** 441–445.

Zatman, S., Gordon, R.G. & Richards, M.A., 2001. Analytical models for the dynamics of diffuse oceanic plate boundaries, *Geophys. J. Int.,* **145,** 145–156.